Synthesis and Characterization of the Heptanuclear $[Mn_6^{III}Co^{III}]^{3+}$ Triplesalen Complex: Evidence for Exchange Pathways Involving Low-spin Co^{III}

Erich Krickemeyer[a], Veronika Hoeke[a], Anja Stammler[a], Hartmut Bögge[a], Jürgen Schnack[b], and Thorsten Glaser[a]

[a] Fakultät für Chemie, Universität Bielefeld, Universitätsstraße 25, 33615 Bielefeld, Germany
[b] Fakultät für Physik, Universität Bielefeld, Universitätsstraße 25, 33615 Bielefeld, Germany

Reprint requests to Prof. Dr. Thorsten Glaser. Fax: +49-(0)521-106-6003.
E-mail: thorsten.glaser@uni-bielefeld.de

Dedicated to Professor Rolf W. Saalfrank on the occasion of his 70th birthday

The reaction of the *tert*-butyl-substituted triplesalen ligand H_6talen$^{t\text{-Bu}_2}$ with $Mn^{II}(OAc)_2 \cdot 4H_2O$ and $K_3[Co^{III}(CN)_6]$ results in the formation of the heptanuclear complex $[\{(talen^{t\text{-Bu}_2})$-$(Mn^{III}(MeOH))_3\}_2\{Co^{III}(CN)_6\}](PF_6)_2(OAc) \cdot 11MeOH$ ($[\mathbf{Mn_6^{III}Co^{III}}](PF_6)_2(OAc) \cdot 11MeOH$, **1** $\cdot 11MeOH$), which has been characterized by FT-IR spectroscopy, elemental analysis, ESI-MS, single-crystal X-ray diffraction, and magnetic measurements. The molecular structure of the $[\mathbf{Mn_6^{III}Co^{III}}]^{3+}$ complex is closely related to the already published analogs $[\mathbf{Mn_6^{III}Cr^{III}}]^{3+}$ and $[\mathbf{Mn_6^{III}Fe^{III}}]^{3+}$. Variable-temperature variable-field and μ_{eff} *vs.* T magnetic data have been analyzed in detail by full-matrix diagonalization of the appropriate spin-Hamiltonian consisting of isotropic exchange, zero-field splitting, and Zeeman interaction, taking into account the relative orientation of the **D** tensors. This allowed a careful inspection of the Mn^{III}-Mn^{III} exchange interaction involving a diamagnetic central metal ion. A satisfactory reproduction of the magnetic data required the incorporation not only of an exchange interaction between the Mn^{III} ions belonging to one triplesalen half unit, but also of an exchange coupling between Mn^{III} ions belonging to different triplesalen subunits. Satisfactory reproduction of the experimental data has been obtained for the parameter set $J_1 = -(0.50 \pm 0.04)$ cm^{-1}, $J_2 = +(0.05 \pm 0.02)$ cm^{-1}, and $D = -(2.5 \pm 0.5)$ cm^{-1}. A detailed analysis of the J_1 coupling taking into account the molecular structures of the three available heptanuclear complexes $[\mathbf{Mn_6^{III}M^{III}}]^{3+}$ (M = Cr, Fe, Co) indicates that the exchange interaction between the Mn^{III} ions belonging to the same triplesalen subunit involves not only an exchange pathway through the central phloroglucinol unit but also an exchange pathway through the central metal ion.
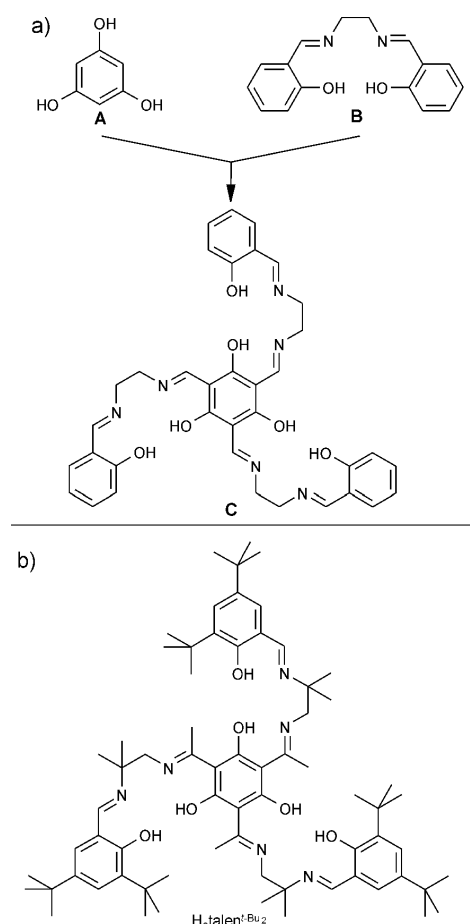
Key words: Magnetic Properties, Heteronuclear Complexes, Exchange Pathways

Introduction

The design and synthesis of molecule-based magnets has attracted considerable interest over the past decades [1 – 3]. Beyond the synthesis of magnetic materials based on molecular entities that exhibit a spontaneous long-range ferromagnetic ordering, the observation that the molecular complex $[Mn_{12}O_{12}(O_2CCH_3)_{16}(OH_2)_4]$, **Mn$_{12}$** [4], exhibits a hysteresis in the magnetization of purely molecular origin [5, 6] opened the field to a new class of molecular magnetic materials called single-molecule magnets (SMMs) [7 – 10]. SMMs possess a superior property in comparison to other paramagnetic polynuclear transition metal complexes: SMMs can be magnetized and retain their polarization in the absence of an external magnetic field. Accordingly, they exhibit a hysteresis in the magnetization in analogy to solid-state magnets. Due to these promising properties, SMMs have attracted a great deal of research attention since their discovery in 1993.

The origin of the slow relaxation of the magnetization at low temperatures is an energy barrier for spin reversal. This energy barrier originates from a

Scheme 1. a) The C_3-symmetric hybrid ligand triplesalen **C** comprised of phloroglucinol **A** for ferromagnetic coupling and salen units **B** for single-site magnetic anisotropy; b) the triplesalen ligand H$_6$talen$^{t\text{-}Bu_2}$ used in this study.

ground state with large total spin S_t and large magnetic anisotropy with an easy axis of magnetization (phenomenologically parameterized by a negative zero-field splitting parameter D). In order to prevent quantum tunnelling through this anisotropy barrier, the rhombicity E/D of the spin should vanish.

In order to match these requirements for SMMs, we have designed the C_3-symmetric triplesalen ligand **C** (Scheme 1a) [11, 12] which combines the 1,3,5-trihydroxybenzene (phloroglucinol) bridging unit **A** [13–19] for ferromagnetic couplings by the spin-polarization mechanism [17, 20–26] and thus high-spin ground states with the coordination environment of a salen ligand **B** for a pronounced magnetic anisotropy [27–29]. We have shown for a series of trinuclear triplesalen complexes of the
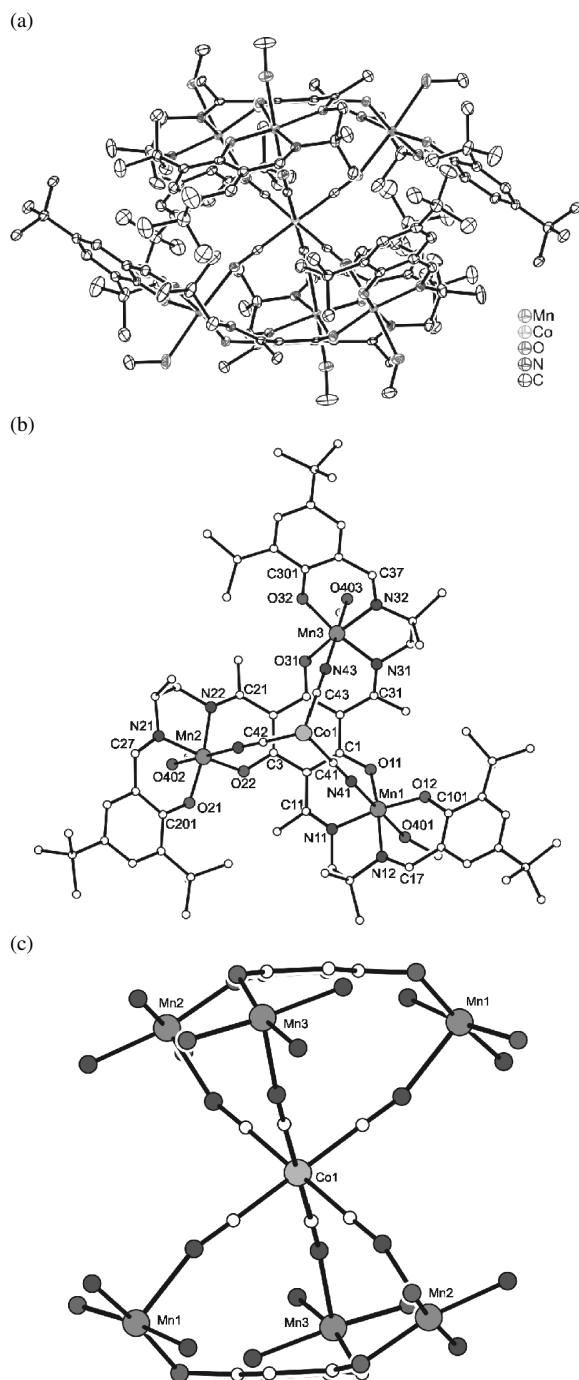
ligand H$_6$talen$^{t\text{-}Bu_2}$ (Scheme 1b) that (*i*) the C_3 symmetry of the triplesalen ligand is impeded onto the complexes and (*ii*) a severe ligand folding occurs in [(talen$^{t\text{-}Bu_2}$)M$_3$] (M = Cu, Ni) resulting in an overall bowl-shaped molecular structure [12, 15]. An advantage of the ligand folding in the trinuclear complexes [(talen$^{t\text{-}Bu_2}$){M(solv)$_n$}$_3$]$^{m+}$ is the pre-organization of the three metal ions for coordination of three facial nitrogen atoms of a hexacyanometallate [M(CN)$_6$]$^{n-}$. Thus, reaction of the molecular building block [(talen$^{t\text{-}Bu_2}$){Mn^{III}(solv)$_n$}$_3$]$^{3+}$ – formed *in situ* by reaction of H$_6$talen$^{t\text{-}Bu_2}$ with Mn^{II}(OAc)$_2$·4H$_2$O – with [Cr(CN)$_6$]$^{3-}$ and [Fe(CN)$_6$]$^{3-}$ resulted in the formation of the heptanuclear complexes [{(talen$^{t\text{-}Bu_2}$)Mn^{III}$_3$}$_2${Cr^{III}-(CN)$_6$}]$^{3+}$ ([**Mn**$_6^{III}$**Cr**^{III}]$^{3+}$) [30] and [{(talen$^{t\text{-}Bu_2}$)-Mn^{III}$_3$}$_2${Fe^{III}(CN)$_6$}]$^{3+}$ ([**Mn**$_6^{III}$**Fe**^{III}]$^{3+}$) [31], respectively (note that the weakly bound solvent molecules on the sixth coordination sites of some of the Jahn-Teller-distorted Mn^{III} ions have been neglected in this formulation). We could (*i*) show that [**Mn**$_6^{III}$**Cr**^{III}]$^{3+}$ is an SMM and [**Mn**$_6^{III}$**Fe**^{III}]$^{3+}$ is not an SMM, and (*ii*) relate this different behavior to differences in the exchange coupling constants of the Mn^{III} ions and the central metal ion.

Here, we present the synthesis and characterization of the heptanuclear complex [{(talen$^{t\text{-}Bu_2}$)Mn^{III}$_3$}$_2$-{Co^{III}(CN)$_6$}]$^{3+}$ ([**Mn**$_6^{III}$**Co**^{III}]$^{3+}$), which is the first member of the heptanuclear triplesalen complex family with a diamagnetic central metal ion. The detailed magnetic characterization and analysis provides insight into the interaction between the Mn^{III} ions.

Results and Analysis

Synthesis and characterization

The reaction of H$_6$talen$^{t\text{-}Bu_2}$, Mn^{II}(OAc)$_2$·4H$_2$O, and K$_3$[Co^{III}(CN)$_6$] in the molar ratio 2 : 6 : 1 in methanolic solution yields dark-brown crystals after addition of NaPF$_6$. The FT-IR spectrum exhibits the characteristic features of the [(talen$^{t\text{-}Bu_2}$)Mn^{III}$_3$]$^{3+}$ building block as found in several other complexes [30, 32–34]. The band at 845 cm^{-1} confirms the presence of PF$_6^-$, while a prominent band at 2155 cm^{-1} can be assigned to the symmetric ν(C≡N) vibration of the [Co^{III}(CN)$_6$]$^{3-}$ unit. The shift from 2128 cm^{-1} in K$_3$[Co^{III}(CN)$_6$] proves the symmetric bridging mode of the [Co^{III}(CN)$_6$]$^{3-}$ anion in [**Mn**$_6^{III}$**Co**^{III}]$^{3+}$. The ESI mass spectrum exhibits a prominent ion at a mass to charge ratio m/z of 918.2 with mass

(a)

(b)

(c)

and isotope distribution patterns corresponding to [**Mn₆Co**]³⁺. The dication [**Mn₆Co**]²⁺ and the monocation [**Mn₆Co**]⁺ exhibit weak signals at 1377.4 and 2753.8, respectively. These data are all consistent with the successful formation of [**Mn**$_6^{III}$**Co**^{III}]³⁺.

⟵ Fig. 1. a) ORTEP plot of the trication [{(talen$^{t\text{-Bu}_2}$)-(Mn^{III}(MeOH))₃}₂{Co^{III}(CN)₆}]³⁺ in crystals of **1**·11MeOH; b) molecular structure of the asymmetric unit in crystals of **1**·11MeOH and numbering scheme used (anions, non-coordinated solvent molecules, and hydrogen atoms omitted for clarity, displacement ellipsoids at the 50 % probability level); c) central core of the trication in **1**.

Single-crystal X-ray diffraction established the formulation [{(talen$^{t\text{-Bu}_2}$)(Mn^{III}(MeOH))₃}₂{Co^{III}(CN)₆}]-(PF₆)₂(OAc)·11MeOH (**1**·11MeOH).

Structural characterization

1·11CH₃OH crystallizes in the space group $P2_1/n$. The asymmetric unit consists of half of the molecule. The other half of the molecule is generated by a crystallographic center of inversion, which is located at the central cobalt ion. The molecular structure of the trication [{(talen$^{t\text{-Bu}_2}$)(Mn^{III}(CH₃OH))₃}₂-{Co^{III}(CN)₆}]³⁺ ([**Mn**$_6^{III}$**Co**^{III}]³⁺) (Fig. 1, Table 1) closely resembles those of [**Mn**$_6^{III}$**Cr**^{III}]³⁺ [30] and [**Mn**$_6^{III}$**Fe**^{III}]³⁺ [31]. Two trinuclear Mn^{III} triplesalen building blocks are connected by the [Co^{III}(CN)₆]³⁻ bridging unit. The Mn^{III} ions are in an axially elongated octahedral environment. Each Mn^{III} is coordinated by two imine nitrogen atoms and two phenolate oxygen atoms of a triplesalen ligand compartment. The coordination environment is completed by a nitrogen atom of the [Co^{III}(CN)₆]³⁻ unit and an oxygen atom of a coordinated methanol molecule. The mean values for the Mn–O bond lengths for the central PhO⁻ and the terminal PhO⁻ are 1.89 and 1.88 Å, respectively, while the mean Mn–N bond length is 1.98 Å for both the central and the terminal imine donors. These values are in accord with [**Mn**$_6^{III}$**Cr**^{III}]³⁺ [30] and [**Mn**$_6^{III}$**Fe**^{III}]³⁺ [31]. The Mn^{III} Jahn-Teller axes point along the N$^{C≡N}$···O^{MeOH} directions, as evidenced by longer mean Mn–N$^{C≡N}$ and Mn–O^{MeOH} bonds of 2.21 and 2.37 Å, respectively.
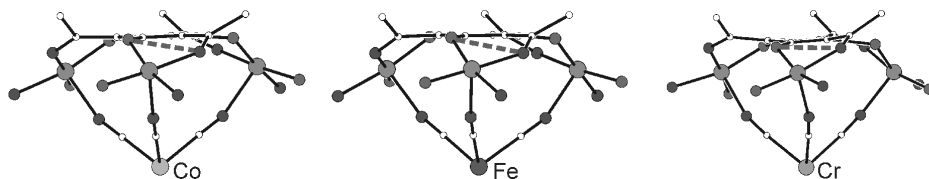
The cobalt ion is coordinated octahedrally by the six carbon atoms of the six bridging cyanide ligands. The mean Co–C bond length of 1.90 Å is smaller in comparison to that of [**Mn₆Cr**]³⁺ (2.07 Å) [30] and [**Mn₆Fe**]³⁺ (1.93 Å) [31]. In accordance with the other heptanuclear triplesalen complexes, the mean ∠(Co–C–N) angle is almost linear (178.9°) whereas the mean ∠(C–N–Mn) angle is bent (163.1°). This bending does not occur randomly but all six C≡N–Mn units bend towards the molecular C_3 axis.

Table 1. Selected interatomic distances (Å) and angles (deg) in **1**·11MeOH[a].

Mn1–O11	1.891(2)	Mn1–O12	1.880(2)	Mn1–N11	1.984(3)	Mn1–N12	1.982(3)
Mn1–N41	2.210(3)	Mn1–O401	2.377(3)	Mn2–O21	1.867(2)	Mn2–O22	1.897(2)
Mn2–N21	1.986(3)	Mn2–N22	1.984(3)	Mn2–N42	2.214(3)	Mn2–O402	2.334(2)
Mn3–O31	1.893(2)	Mn3–O32	1.884(2)	Mn3–N31	1.983(3)	Mn3–N32	1.986(3)
Mn3–N43	2.207(3)	Mn3–O403	2.389(2)	Co1–C42	1.900(3)	Co1–C41	1.902(3)
Co1–C43	1.903(3)	O11–C1	1.311(4)	O12–C101	1.322(4)	O21–C201	1.315(4)
O22–C3	1.312(4)	O31–C5	1.318(4)	O32–C301	1.314(4)	N11–C11	1.300(4)
N12–C17	1.293(4)	N21–C27	1.278(4)	N22–C21	1.289(4)	N31–C31	1.308(4)
N32–C37	1.288(4)	Mn1–Mn2	6.803(2)	Mn1–Mn3	6.7499(15)	Mn2–Mn3	6.7808(15)
Mn1–Co1	5.2160(10)	Mn2–Co1	5.2080(11)	Mn3–Co1	5.2038(14)		

O12–Mn1–O11	96.00(10)	O12–Mn1–N12	91.91(11)	O11–Mn1–N12	168.34(11)	O12–Mn1–N11	171.07(10)
O11–Mn1–N11	88.00(10)	N12–Mn1–N11	83.02(11)	O12–Mn1–N41	95.99(10)	O11–Mn1–N41	90.83(10)
N12–Mn1–N41	96.87(11)	N11–Mn1–N41	91.92(11)	O12–Mn1–O401	86.00(10)	O11–Mn1–O401	86.11(10)
N12–Mn1–O401	85.91(11)	N11–Mn1–O401	86.31(11)	N41–Mn1–O401	176.51(10)	O21–Mn2–O22	95.65(9)
O21–Mn2–N22	171.74(10)	O22–Mn2–N22	89.23(10)	O21–Mn2–N21	91.22(10)	O22–Mn2–N21	169.57(10)
N22–Mn2–N21	83.08(11)	O21–Mn2–N42	95.40(10)	O22–Mn2–N42	89.46(10)	N22–Mn2–N42	91.31(11)
N21–Mn2–N42	97.71(11)	O21–Mn2–O402	89.02(10)	O22–Mn2–O402	84.22(9)	N22–Mn2–O402	84.83(10)
N21–Mn2–O402	88.07(10)	N42–Mn2–O402	172.63(10)	O32–Mn3–O31	95.79(9)	O32–Mn3–N31	170.62(11)
O31–Mn3–N31	88.15(10)	O32–Mn3–N32	91.55(10)	O31–Mn3–N32	168.00(10)	N31–Mn3–N32	83.23(11)
O32–Mn3–N43	95.20(10)	O31–Mn3–N43	89.83(10)	N31–Mn3–N43	93.32(11)	N32–Mn3–N43	98.97(11)
O32–Mn3–O403	86.53(10)	O31–Mn3–O403	86.18(9)	N31–Mn3–O403	85.25(10)	N32–Mn3–O403	84.80(10)
N43–Mn3–O403	175.79(9)	C42#1–Co1–C42	179.997(1)	C42–Co1–C41#1	88.94(13)	C42–Co1–C41	91.06(13)
C41#1–Co1–C41	180.00(16)	C42–Co1–C43	91.19(13)	C41–Co1–C43	89.95(13)	C42–Co1–C43#1	88.81(13)
C41–Co1–C43#1	90.05(13)	C43–Co1–C43#1	179.999(1)				

[a] Symmetry transformations used to generate equivalent atoms: #1 $-x+1, -y+1, -z+1$.
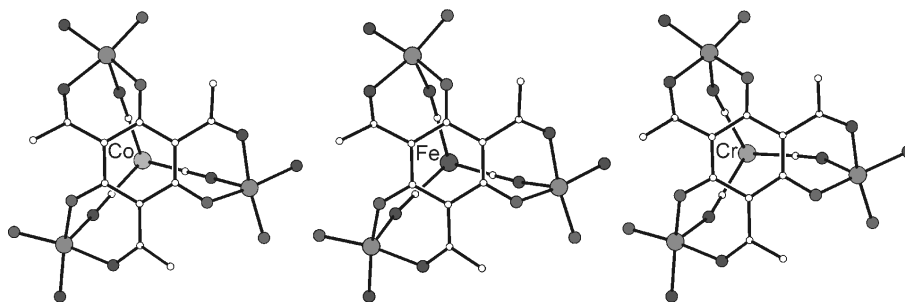
a)

b)

Fig. 2. Sections of the molecular structures of [Mn$_6^{III}$Co^{III}]$^{3+}$ (left), [Mn$_6^{III}$Fe^{III}]$^{3+}$ [31] (center), and [Mn$_6^{III}$Cr^{III}]$^{3+}$ [30] (right) with the view direction in the benzene plane of the central phloroglucinol (a) and perpendicular to this plane (b). The dashed lines in (a) represent the vector defined by O^{Ph}-N^{ketimine} to visualize the angle between this vector and the central benzene plane.

An important aspect for the Mn-Mn exchange interaction is the exact structure of the trinuclear triplesalen building block. We have applied several parameters for a quantitative description of the ligand folding in the study of the trinuclear triplesalen com-

plexes [12, 15]. It turned out that the best parameters to quantitatively describe the ligand folding are the bent angles $\varphi^{central}$ and $\varphi^{terminal}$. The bent angle φ is defined by $\varphi = 180° - \angle(M\text{–}X_{NO}\text{–}X_R)$ (X_{NO}, midpoint of adjacent N and O donor atoms; X_R, mid-

point of the six-membered chelate ring containing the N and O donor atoms) [35]. This bent angle is best suited to differentiate between a bending along an idealized line through neighboring N and O ligands and a line perpendicular to the former, resulting in a helical distortion of the salen subunit. In the trinuclear Ni^{II} and Cu^{II} complexes, $\varphi^{central}$ is in the range of $20-30°$ while $\varphi^{terminal}$ is significantly smaller in the range of $3-9°$. Coordination of the hexacyanometallate increases the bent angle $\varphi^{central}$ to $36.0°$ in $[Mn_6^{III}Fe^{III}]^{3+}$ [31], $46.7°$ in $[Mn_6^{III}Cr^{III}]^{3+}$ [30], and $38.1°$ in $[Mn_6^{III}Co^{III}]^{3+}$. The terminal bent angle is still small with 7.9, 8.5, and $10.0°$ for $[Mn_6^{III}Fe^{III}]^{3+}$, $[Mn_6^{III}Cr^{III}]^{3+}$, and $[Mn_6^{III}Co^{III}]^{3+}$, respectively. The larger $\varphi^{central}$ for $[Mn_6^{III}Cr^{III}]^{3+}$ correlates with the longer Cr–C bond of 2.07 Å in comparison to 1.93 Å in $[Mn_6^{III}Fe^{III}]^{3+}$ and 1.90 Å in $[Mn_6^{III}Co^{III}]^{3+}$.

As the simple assumption that a smaller hexacyanometallate unit forces the triplesalen unit to bend more does not hold, we have identified a stronger helical distortion in $[Mn_6^{III}Fe^{III}]^{3+}$ in comparison to $[Mn_6^{III}Cr^{III}]^{3+}$ [31]. This distortion may be best visualized by the angle between the benzene plane of the central phloroglucinol and the vector formed by the central phenolate oxygen atom and the central ketimine nitrogen atom (Fig. 2a). This angle is only $1.3°$ in $[Mn_6^{III}Cr^{III}]^{3+}$ [30], whereas it is $11.7°$ in $[Mn_6^{III}Fe^{III}]^{3+}$ [31] and $9.0°$ in $[Mn_6^{III}Co^{III}]^{3+}$. The stronger helical distortion in $[Mn_6^{III}Co^{III}]^{3+}$ and $[Mn_6^{III}Fe^{III}]^{3+}$ comes along with a slighter distortion of the central phloroglucinol ring and its six direct substituents. These twelve atoms are all in an idealized plane, whereas in $[Mn_6^{III}Cr^{III}]^{3+}$ the three oxygen atoms lie below the plane, and the three ketimine carbon atoms lie above the plane (Fig. 2a).

Magnetic measurements

Temperature-dependent magnetic susceptibility measurements $(2-290$ K, 0.1 T) on powdered samples of $\mathbf{1}\cdot 7H_2O$ reveal $\mu_{eff} = 11.88$ μ_B at 290 K, which decreases monotonically with temperature to a minimum of 6.52 μ_B at 1.9 K (Fig. 3a). The room temperature value is close to the spin-only value of 12.0 μ_B of six uncoupled Mn^{III} high-spin ions ($S_i = 2$, $g_i = 2.0$). The continuous decrease of μ_{eff} indicates dominating antiferromagnetic interactions between the Mn^{III} ions. In order to probe the magnetic anisotropy, we have performed variable-temperature variable-field (VTVH) magnetization measurements

for $\mathbf{1}\cdot 7H_2O$ at 1, 4, and 7 T (Fig. 3b). The iso-field lines exhibit a strong nesting behavior which is indicative of strong magnetic anisotropy [36]. The saturation magnetization at the highest field of 7 T is 16.78 μ_B.

In order to obtain some quantitative insight into magnitudes and ratios of the exchange couplings J_{ij} and zero-field splittings D_i, we have performed a full-matrix diagonalization of the appropriate spin-Hamiltonian including isotropic HDvV exchange, zero-field splitting, and Zeeman interaction (see Experimental Section for details). A frequently used simplification in such spin-Hamiltonians is a collinearity of the local **D** tensors, which is not always the case. We have incorporated the zero-field splitting for the Mn^{III} ions including the relative orientations of the individual **D** tensors by the angle θ of the Jahn-Teller axes with the molecular axis.

As the central metal ion is a diamagnetic low-spin Co^{III} ion, our first coupling scheme only incorporated the Mn^{III}-Mn^{III} exchange interaction J_1 (Fig. 4a) of Mn^{III} ions belonging to the same trinuclear triplesalen building block. Using this coupling scheme, we have not been able to satisfactorily reproduce both experimental data sets, the temperature dependence of μ_{eff} and the results of the VTVH measurements. The temperature dependence of μ_{eff} required a coupling constant J_1 of about -0.5 cm^{-1} without providing a good reproduction of the experimental data. Contrarily, the VTVH data indicated a weaker coupling. However, no satisfactory reproduction of the VTVH data was possible. The iso-field lines at 4 and 7 T could be reproduced qualitatively. The 1 T data could not even qualitatively be reproduced as the simulations exhibited saturation behavior whereas the experimental data do not.

As the chosen coupling scheme did not provide a reasonable reproduction of the experimental data, our next approach was to take into account a coupling of Mn^{III} ions belonging to different trinuclear triplesalen subunits. However, a consideration of the full S_6 symmetry would require incorporation of two additional coupling constants, *e. g.* S_1 couples with S_4 (J_{14}) and equally with S_5 and S_6 ($J_{15} = J_{16}$). As the incorporation of two additional coupling constants between the building blocks would overparametrize the system, we arbitrarily have chosen to incorporate only the exchange coupling between a spin on one building block and the spin of the other building block in *trans* position, *i. e.* $J_{14} \equiv J_2$. The two *cis* pathways have been neglected. This results in the coupling scheme provided in Fig. 4b. Using this improved coupling scheme,
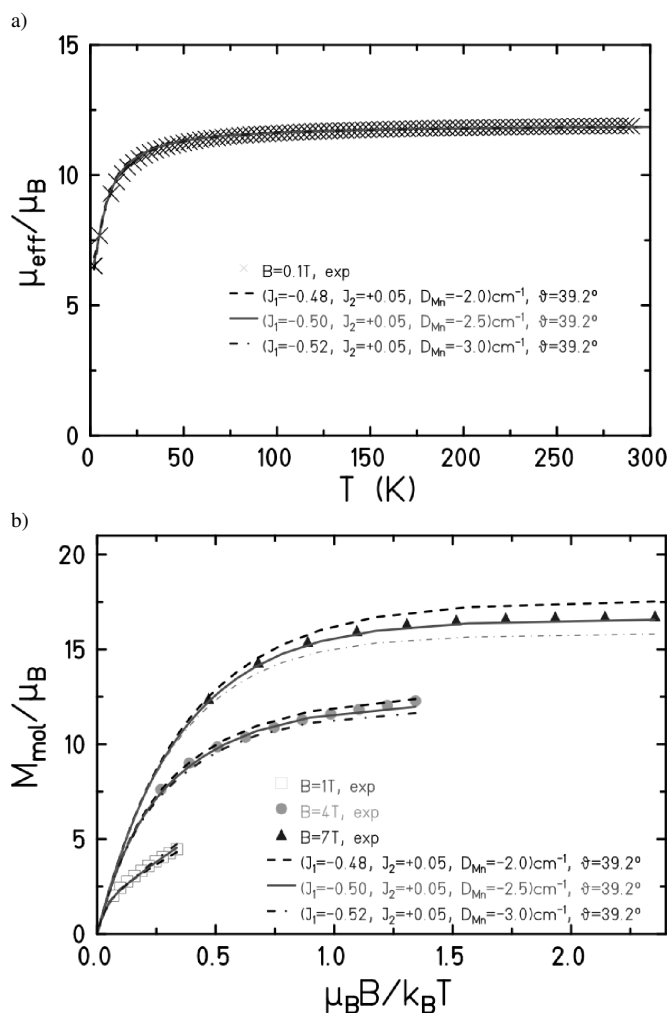
a)

b)

Fig. 3. a) Temperature dependence of μ_{eff} at 0.1 T and b) VTVH at 1, 4, and 7 T for **1**·7H$_2$O. The lines correspond to simulations based on the complete spin-Hamiltonian by full matrix diagonalization. The simulations provided are a selection of a thorough search in the J_1, J_2, and D parameter space.
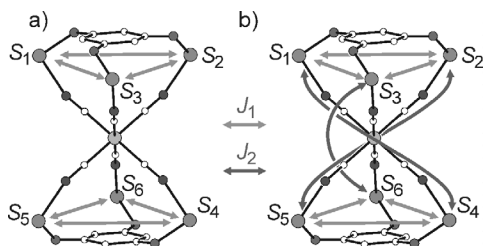

Fig. 4. a) Coupling schemes for the analysis of the magnetic data using only the Mn^{III}-Mn^{III} exchange interaction between the ions of the same trinuclear triplesalen subunit (J_1) and b) including one exchange pathway for the *trans* Mn^{III} ion in the other trinuclear triplesalen subunit (J_2).

we have performed an intensive search in the J_1, J_2, and D parameter space. The μ_{eff} *vs. T* data prove to be highly insensitive to the zero-field splitting. Tak-

ing into account a slightly ferromagnetic J_2 interaction yielded a good reproduction of the experimental temperature dependence. More sensitive to a change of all three parameters are the VTVH data. Especially the curvature of the 1 T data set has only been reproduced by taking into account a ferromagnetic coupling constant of +0.05 cm^{-1} for J_2. Evaluating the whole parameter search, the best values are given by J_1 = $-(0.50\pm0.04)$ cm^{-1}, J_2 = $+(0.05\pm0.02)$ cm^{-1}, and D = $-(2.5\pm0.5)$ cm^{-1}. A limited number of simulations is incorporated in Fig. 3.

Discussion

The detailed analysis of the experimental magnetic data suggests a Mn^{III}-Mn^{III} coupling constant within a trinuclear triplesalen subunit of only J_1 =

-0.50 cm^{-1}. This coupling is significantly weaker in comparison to $J_1 = -1.03$ cm^{-1} in [Mn$_6^{III}$Cr^{III}]$^{3+}$ [30] and $J_1 = -0.85$ cm^{-1} in [Mn$_6^{III}$Fe^{III}]$^{3+}$ [31]. In other trinuclear Mn^{III} triplesalen subunits the following Mn^{III}-Mn^{III} coupling constants have been established: $J = -0.30$ cm^{-1} in [(talen^{NO_2}){Mn^{III}(DMSO)$_2$}$_3$]-(ClO$_4$)$_3$ [37], $J = -0.70$ cm^{-1} in [{(talen$^{t-Bu_2}$)(Mn^{III}-(MeOH))$_3$}{(Me$_3$tacn)Cr^{III}(CN)$_3$}](ClO$_4$)$_3$ [33] and $J = -0.60$ cm^{-1} in {[{(talen$^{t-Bu_2}$)Mn$_3$(MeOH)}$_2$(μ_2-OAc)$_3$](μ_2-OAc)}$_n$(BPh$_4$)$_{2n}$ [34].

This comparison indicates that the Mn^{III}-Mn^{III} coupling depends on steric and electronic effects. However, in the series of heptanuclear complexes of the *tert*-butyl-substituted ligand H$_6$talen$^{t-Bu_2}$, the coupling in [Mn$_6^{III}$Co^{III}]$^{3+}$ is relatively weak. We have tried to relate the differences between the coupling constants to structural differences. As analyzed in the previous section, the helical distortion in [Mn$_6^{III}$Co^{III}]$^{3+}$ is close to that found in [Mn$_6^{III}$Fe^{III}]$^{3+}$, and significantly stronger than that found in [Mn$_6^{III}$Cr^{III}]$^{3+}$. Therefore, the coupling constant in [Mn$_6^{III}$Cr^{III}]$^{3+}$ should be exceptional within this series and not the coupling constant in [Mn$_6^{III}$Co^{III}]$^{3+}$, as found experimentally. We have compared more structural parameters (distances, angles, torsion angles), finding that the molecular structures of [Mn$_6^{III}$Co^{III}]$^{3+}$ and [Mn$_6^{III}$Fe^{III}]$^{3+}$ are almost super-imposable (Fig. 2b) due to the same size of the central hexacyanometallate unit. Therefore, it might be reasonable to assume that the difference in the coupling constant between these two complexes is of electronic nature.

As we have found some influence on the experimental magnetic data of the long-range coupling J_2 from one building block to the other, facilitated by the exchange pathway Mn^{III}–C≡N–Co^{III}–C≡N–Mn^{III}, it might be possible that there is an exchange pathway not only between Mn^{III} ions of two different trinuclear building blocks but also of the same building block through the central diamagnetic Co^{III} ion. That would result in two independent exchange pathways for one Mn^{III}-Mn^{III} coupling constant J_1: one pathway through the central phloroglucinol unit and one pathway through the central metal ion. The latter should depend on the electron configuration of the central metal ion which is d^6 l. s. in [Mn$_6^{III}$Co^{III}]$^{3+}$ and d^5 l. s. in [Mn$_6^{III}$Fe^{III}]$^{3+}$.

In conclusion, the synthesis, structural and magnetic characterization of [{(talen$^{t-Bu_2}$)(Mn^{III}(MeOH))$_3$}$_2$-{Co^{III}(CN)$_6$}]$^{3+}$ provides evidence for a Mn^{III}-Mn^{III} exchange interaction through the central metal ion. In order to test this working hypothesis, we will carefully analyze more members of this family of heptanuclear triplesalen complexes.

Experimental Section

Preparation of compounds

A solution of H$_6$talen$^{t-Bu_2}$ (222 mg, 0.200 mmol) and Mn^{II}(OAc)$_2$·4H$_2$O (147 mg, 0.600 mmol) was heated at reflux in CH$_3$OH (75 mL) for 20 min. The resulting dark-brown solution was cooled to r. t. and filtered. The filtrate was treated with a solution of K$_3$[Co^{III}(CN)$_6$] (33 mg, 0.099 mmol) and 18-crown-6 (200 mg, 0.767 mmol) in CH$_3$OH (25 mL) and stirred for 30 min. After addition of a solution of NaPF$_6$ (70 mg, 0.417 mmol) and 18-crown-6 (200 mg, 0.767 mmol) in CH$_3$OH (25 mL), stirring was continued for further 15 min. The resulting solution was filtered using very fine filter paper (Blauband). Slow evaporation of the filtrate caused the deposition of dark-brown crystals, which were separated, washed twice with cold MeOH/H$_2$O (1 : 1), and air-dried. The sample used for magnetic measurements was analyzed as [{(talen$^{t-Bu_2}$)(Mn(MeOH))$_3$}$_2${Co(CN)$_6$}](PF$_6$)$_2$-(OAc)·7H$_2$O. Yield: 172 mg (25 %). – IR (KBr): ν = 2955, 2906, 2870, 2155 (C≡N), 1613, 1570, 1535, 1493, 1275, 845, 575, 554 cm^{-1}. – MS ((+)-ESI, MeOH): m/z = 918.2 [Mn$_6$Co]$^{3+}$, 1377.4 [Mn$_6$Co]$^{2+}$, 2753.8 [Mn$_6$Co]$^+$. – C$_{152}$H$_{233}$N$_{18}$O$_{27}$P$_2$F$_{12}$Mn$_6$Co (3423.12): calcd. C 53.33, H 6.86, N 7.37; found C 53.08, H 6.40, N 7.23.

X-Ray crystallographic data collection and refinement

Crystal data for **1**·11MeOH: M = 3649.42 g mol^{-1}, C$_{163}$H$_{263}$CoF$_{12}$Mn$_6$N$_{18}$O$_{31}$P$_2$, monoclinic, space group $P2_1/n$, a = 18.594(4), b = 25.628(5), c = 19.504(4) Å, β = 93.89(3)°, V = 9273(3) Å^3, Z = 2, ρ = 1.31 g cm^{-3}, μ = 0.6 mm^{-1}, $F(000)$ = 3860, crystal size = 0.40 × 0.20 × 0.11 mm^3. Crystals of **1**·11MeOH were removed from the mother liquor and immediately cooled to 100(2) K on a Nonius KappaCCD diffractometer (four circle goniometer, MoK_α radiation, graphite monochromator, detector distance 35.90 mm). A total of 116546 reflections (2.16 < θ < 25.00°) were collected of which 16270 reflections were unique (R_{int} = 0.0605). An empirical absorption correction using equivalent reflections was performed with the program SADABS 2.10 [38]. The structure was solved with SHELXS-97 [39] and refined using SHELXL-97 [39] to R = 0.0538 for 12996 reflections with $I \geq 2\sigma(I)$, R = 0.0711 for all reflections; Max/min residual electron density 1.00 and -1.00 e Å^{-3}. All F atoms of the PF$_6^-$ anion were located and refined on two positions. The OH hydrogen atoms of solvent MeOH molecules were not located. The acetate anion was found disordered with a MeOH molecule at a center of inversion. The unit cell contains four voids with a vol-

ume of approx. 130 Å^3. Originally, two disordered MeOH molecules were found in the region of each void, but could not be refined properly. Thus, their scattering power was removed from the data set using the PLATON/SQUEEZE routine [40]. They are, however, included in the given sum formula.

CCDC 753929 contains the supplementary crystallographic data for this paper. These data can be obtained free of charge from The Cambridge Crystallographic Data Centre *via* www.ccdc.cam.ac.uk/data_request/cif.

Other physical measurements

Temperature-dependent magnetic susceptibilities were measured on powdered samples by using a SQUID magnetometer (Quantum Design MPMS XL-7 EC) at 0.1 T (2 – 290 K). VTVH measurements were performed at 1, 4, and 7 T in the range 2 – 10 K with the magnetization equidistantly sampled on a $1/T$ temperature scale. For calculation of the molar magnetic susceptibilities, χ_M, the measured susceptibilities were corrected for the underlying diamagnetism of the sample holder and the sample by using tabulated Pascal's constants. Infrared spectra (400 – 4000 cm^{-1}) of solid samples were recorded on a Shimadzu FT-IR 8300 instrument from KBr disks. ESI mass spectra were recorded on an Esquire 3000 ion trap mass spectrometer (Bruker Daltonik GmbH, Bremen, Germany).

Computational details

The magnetic properties of [**Mn$_6^{III}$Co^{III}**]$^{3+}$ were simulated by a full-matrix diagonalization of the spin-Hamiltonian in Eq. 1.

$$\hat{H} = -2\sum_{i<j} J_{ij}\hat{S}_i \cdot \hat{S}_j + \sum_i D_i(\hat{S}_i \cdot e_i(\vartheta_i \varphi_i))^2$$
$$+ \mu_B \sum_i \mathbf{B} \cdot \underset{=i}{\mathbf{g}} \cdot \hat{S}_i \qquad (1)$$

Here the first sum reflects the isotropic exchange interaction between spins given by the spin vector operators $\hat{S}_i$ at sites i. A negative value of J_{ij} corresponds to an antiferromagnetic coupling. The anisotropic magnetization behavior of the manganese ions is accounted for by local anisotropy tensors in the second sum. The tensors are parameterized by a strength factor $D_i = D$, which is the same for all six manganese ions. The local unit vector e_i, which is parameterized by the polar angles ϑ_i and φ_i, points along the local Jahn-Teller axis and represents an easy or a hard axis depending on the sign of D. Due to the S_6 symmetry all six local unit vectors e_i can be parameterized by the common polar angle between the Jahn-Teller axis and the S_6 symmetry axis, which is $\vartheta = 39.2°$. The relative φ_i angles are determined by the S_6 symmetry. The third term models the interaction with the applied magnetic field. $\underset{=i}{\mathbf{g}}$ represents the local **g**-tensor at site i. For the Mn^{III} ions an isotropic value of 2.0 was assumed.

The Hilbert space of the full spin-Hamiltonian has a dimension of 15625. In the presence of a magnetic field we employed inversion symmetry. This reduced the average matrix size to roughly 7800 × 7800. Since the measurements were performed with powder samples we also employed an orientational average using a Lebedev grid with 50 orientations [41, 42].

[1] J. S. Miller, *Inorg. Chem.* **2000**, *39*, 4392 – 4408.
[2] J. S. Miller, A. J. Epstein in *Molecular Magnetism: From Molecular Assemblies to the Devices*, (Eds.: E. Coronado, P. Delhaes, D. Gatteschi, J. S. Miller), NATO ASI Series, Series E, Vol. 321, Kluwer Academic Publishers, Dordrecht, **1996**, pp. 379 – 414.
[3] J. S. Miller, A. J. Epstein, W. M. Reiff, *Acc. Chem. Res.* **1988**, *21*, 114 – 120.
[4] T. Lis, *Acta Crystallogr.* **1980**, *36*, 2042 – 2046.
[5] R. Sessoli, D. Gatteschi, A. Caneschi, M. A. Novak, *Nature* **1993**, *365*, 141 – 143.
[6] R. Sessoli, H. L. Tsai, A. R. Schake, S. Y. Wang, J. B. Vincent, K. Folting, D. Gatteschi, G. Christou, D. N. Hendrickson, *J. Am. Chem. Soc.* **1993**, *115*, 1804 – 1816.
[7] G. Christou, D. Gatteschi, D. N. Hendrickson, R. Sessoli, *MRS Bull.* **2000**, *25*, 66 – 71.
[8] J. R. Long in *Chemistry of Nanostructured Materials*, (Ed.: P. Yang), World Scientific, Hong Kong, **2003**, pp. 291 – 315.
[9] D. Gatteschi, R. Sessoli, *Angew. Chem.* **2003**, *115*, 278 – 309; *Angew. Chem. Int. Ed.* **2003**, *42*, 268 – 297.
[10] D. Gatteschi, R. Sessoli, J. Villain, *Molecular Nanomagnets*, Oxford University Press, Oxford, **2006**.
[11] T. Glaser, M. Heidemeier, T. Lügger, *Dalton Trans.* **2003**, 2381 – 2383.
[12] T. Glaser, M. Heidemeier, R. Fröhlich, P. Hildebrandt, E. Bothe, E. Bill, *Inorg. Chem.* **2005**, *44*, 5467 – 5482.
[13] T. Glaser, M. Gerenkamp, R. Fröhlich, *Angew. Chem.*

2002, *114*, 3984 – 3986; *Angew. Chem. Int. Ed.* **2002**, *41*, 3823 – 3825.

[14] T. Glaser, M. Heidemeier, S. Grimme, E. Bill, *Inorg. Chem.* **2004**, *43*, 5192 – 5194.

[15] T. Glaser, M. Heidemeier, J. B. H. Strautmann, H. Bögge, A. Stammler, E. Krickemeyer, R. Huenerbein, S. Grimme, E. Bothe, E. Bill, *Chem. Eur. J.* **2007**, *13*, 9191 – 9206.

[16] H. Theil, C.-G. Frhr. v. Richthofen, A. Stammler, H. Bögge, T. Glaser, *Inorg. Chim. Acta* **2008**, *361*, 916 – 924.

[17] T. Glaser, H. Theil, M. Heidemeier, *C. R. Chim.* **2008**, *11*, 1121 – 1136.

[18] V. A. Ung, A. M. W. Cargill Thompson, D. A. Bardwell, D. Gatteschi, J. C. Jeffery, J. A. McCleverty, F. Totti, M. D. Ward, *Inorg. Chem.* **1997**, *36*, 3447 – 3454.

[19] J. A. McCleverty, M. D. Ward, *Acc. Chem. Res.* **1998**, *31*, 842 – 851.

[20] H. C. Longuet-Higgins, *J. Chem. Phys.* **1950**, *18*, 265 – 274.

[21] H. Iwamura, *Adv. Phys. Org. Chem.* **1990**, *26*, 179 – 253.

[22] K. Yoshizawa, R. Hoffmann, *J. Am. Chem. Soc.* **1995**, *117*, 6921 – 6926.

[23] H. Iwamura, N. Koga, *Acc. Chem. Res.* **1993**, *26*, 346 – 351.

[24] D. A. Dougherty, *Acc. Chem. Res.* **1991**, *24*, 88 – 94.

[25] A. A. Ovchinnikov, *Theoret. Chim. Acta* **1978**, *47*, 297 – 304.

[26] T. Glaser, T. Lügger, R. Fröhlich, *Eur. J. Inorg. Chem.* **2004**, 394 – 400.

[27] B. J. Kennedy, K. S. Murray, *Inorg. Chem.* **1985**, *24*, 1552 – 1557.

[28] S. Mitra, *Progr. Inorg. Chem.* **1977**, *22*, 309 – 408.

[29] A. Bencini, I. Ciofini, M. G. Uytterhoeven, *Inorg. Chim. Acta* **1998**, *274*, 90 – 101.

[30] T. Glaser, M. Heidemeier, T. Weyhermüller, R.-D. Hoffmann, H. Rupp, P. Müller, *Angew. Chem.* **2006**, *118*, 6179 – 6183; *Angew. Chem. Int. Ed.* **2006**, *45*, 6033 – 6037.

[31] T. Glaser, M. Heidemeier, E. Krickemeyer, H. Bögge, A. Stammler, R. Fröhlich, E. Bill, J. Schnack, *Inorg. Chem.* **2009**, *48*, 607 – 620.

[32] C. Mukherjee, A. Stammler, H. Bögge, T. Glaser, *Inorg. Chem.* **2009**, *48*, 9476 – 9484.

[33] C.-G. Frhr. v. Richthofen, C.-G., A. Stammler, H. Bögge, M. W. DeGroot, J. R. Long, T. Glaser, *Inorg. Chem.* **2009**, *48*, 10165 – 10176.

[34] T. Glaser, M. Heidemeier, H. Theil, A. Stammler, H. Bögge, J. Schnack, *Dalton Trans.* **2010**, *39*, 192 - 199.

[35] L. Cavallo, H. Jacobsen, *Eur. J. Inorg. Chem.* **2003**, 892 – 902.

[36] J.-J. Girerd, Y. Journaux in *Physical Methods in Bioinorganic Chemistry*; (Ed.: L. J. Que), University Science Books, Sausalito, **2000**, pp. 321 – 374.

[37] T. Glaser, M. Heidemeier, R. Fröhlich, *Compt. Rend. Chim.* **2007**, *10*, 71 – 78.

[38] G. M. Sheldrick, SADABS (version 2.10), Program for Empirical Absorption Correction of Area Detector Data, University of Göttingen, Göttingen (Germany) **2003**.

[39] G. M. Sheldrick, SHELXS/L-97, Programs for Crystal Structure Determination, University of Göttingen, Göttingen (Germany) **1997**. See also: G. M. Sheldrick, *Acta Crystallogr.* **1990**, *A46*, 467 – 473; *ibid.* **2008**, *A64*, 112 – 122.

[40] A. L. Spek, PLATON, A Multipurpose Crystallographic Tool, Utrecht University, Utrecht (The Netherlands) **2000**. See also: A. L. Spek, *J. Appl. Crystallogr.* **2003**, *36*, 7 – 13.

[41] V. I. Lebedev, D. N. Laikov, *Dokl. Akad. Nauk* **1999**, *366*, 741 – 745.

[42] J. Schnack, *Condens. Matter Phys.* **2009**, *12*, 323 – 330.